

# YORP effect with anisotropic radiation

S. Breiter<sup>1</sup>\* and D. Vokrouhlický<sup>2</sup>†

<sup>1</sup>*Astronomical Observatory, A. Mickiewicz University, Słoneczna 36, PL60-286 Poznań, Poland*

<sup>2</sup>*Institute of Astronomy, Charles University, V Holešovičkách 2, 18000 Prague 8, Czech Republic.*

## ABSTRACT

The influence of optical scattering and thermal radiation models on the Yarkovsky-O'Keefe-Radzievskii-Paddack (YORP) effect is studied. Lambertian formulation is compared with Hapke scattering and emission laws and Lommel-Seeliger reflection. Although the form of reflectivity function strongly influences mean torques due to scattering or thermal radiation alone, their combined contribution to the rotation period YORP is not much different from the standard Lambertian values. For higher albedo values the differences between the Hapke and Lambert models become significant for the YORP in attitude.

**Key words:** radiation mechanisms: thermal—methods: numerical—celestial mechanics—minor planets, asteroids: general

## 1 INTRODUCTION

The importance of radiation recoil forces on both orbital motion and rotation of minor bodies in the Solar System has been commonly appreciated over the last decade. The Yarkovsky effect, caused by lagged thermal radiation from the surface of a spinning body (directly detected in the orbital motion of 6489 Golevka (Chesley et al. 2003) and 1992 BF (Vokrouhlický et al. 2008)), has occurred to be the key to the proper understanding of asteroid long-term dynamics. Since the paper of Rubincam (2000), the influence of torques due to radiation recoil is known as the YORP (Yarkovsky-O'Keefe-Radzievskii-Paddack) effect, acknowledging the works of Yarkovsky (1901), Radzievskii (1954), Paddack (1969), and O'Keefe (1976). Unlike the orbital Yarkovsky effect, YORP involves both the scattering of incident light and its thermal re-radiation, and it occurs even for objects with zero conductivity. Direct detections of YORP effect in the rotation of asteroids 54509 YORP (Lowry et al. 2007; Taylor et al. 2007), 1862 Apollo (Kaasalainen et al. 2007), 1620 Geographos (Ďurech et al. 2008), and 3103 Eger (Ďurech et al. 2009), has proved the existence of YORP. On the other hand, however, the agreement between the observed and modeled values in each case can be qualified as merely having a similar order of magnitude and all present YORP models are still simplified and incomplete. What is worse, the failure to detect a theoretically predicted YORP effect for 25143 Itokawa (Ďurech et al. 2008) has helped to realize an extreme sensitivity of these simplified models to the fine details of shape, centre of mass location and spin axis orientation in the body frame (Ďurech et al. 2008; Scheeres & Gaskell 2008; Statler 2009; Breiter et al. 2009).

Most of these models assume that both scattering and thermal radiation is Lambertian, i.e. a photon can be emitted or scattered with equal probability in any direction, hence the exiting

flux is proportional to the cosine of zenith distance according to the projected area of the radiating/scattering surface element. Although Breiter et al. (2007) mentioned a more general scattering model, their work on YORP for spheroids was based on the Lambertian assumption. Scheeres (2007) added a specular reflection to the Lambertian scattering, but such an improvement has no effect on the mean torque, as observed by Rubincam (2000) and proved by Nesvorný & Vokrouhlický (2008) and Rubincam & Paddack (2010). Statler (2009) made a step further, using a hemispheric albedo derived from the scattering model of Hapke (2002) instead of the usual Bond albedo (Vokrouhlický & Bottke 2001). Moreover, the TACO model of Statler for the first time incorporates the important observation that photons bouncing between various surface elements do not produce the net torque until they finally exit into outer space.

The main objective of the present work is to include a non-Lambertian scattering and radiation into the recent YORP model of Breiter et al. (2010) and judge the significance of this improvement. Roughly speaking, a departure from the Lambertian model is essentially caused by interreflections and occlusions. Both phenomena occur at various levels of resolution and one has to be careful about this issue. Out of the two principal scattering models for asteroids surface developed by Lumme & Bowell (1981) and Hapke (Hapke 1981; Hapke & Wells 1981; Hapke 1984, 1986, 2002, 2008) we have chosen the latter. However, both models were created to interpret photometric observations; as such, they attempt to include phenomena happening at various resolution levels that merge in the final integrated brightness. In these circumstances, our present paper focuses on accounting for the regolith grain size ( $< 1$  mm) scale phenomena described by an appropriate part of the Hapke reflectance and emissivity models. It means ignoring the macroscopic roughness corrections and shape-dependent beaming factors. Interreflections occurring between larger surface fragments require a different approach and will be discussed in another article, whereas

\* E-mail: breiter@amu.edu.pl

† E-mail: vokrouhl@cesnet.cz

the large scale occlusions (shadowing) are already incorporated in most of existing YORP models. To a large extent the present contribution has been motivated by the problem of YORP effect on a high albedo asteroid 3103 Eger, where only a convex shape model is available, so larger scale interreflections have to be neglected anyway.

We decided to present a detailed derivation of the radiation recoil force and associated YORP torque using the terminology of modern radiometry instead of traditional astrophysical framework dating back to Chandrasekhar (1950). In this respect we owe much to the collection of Max Fairbairn essays available on-line thanks to J.B. Tatum (<http://orca.phys.uvic.ca/~tatum/plphot.html>).

## 2 SCATTERING AND RADIATION

### 2.1 Irradiance

Consider an infinitesimal element  $dS$  of an atmosphereless celestial body surface. Further, we call  $dS$  a *physical surface*, to distinguish it from a *normal surface* i.e. an infinitesimal surface perpendicular to some specified direction of incident or emitted radiation.

Local solar frame (LSF) will be defined with the origin at the centre of  $dS$ , with  $x$ -axis pointing to the intersection of the meridian passing through the Sun and the horizon plane,  $z$ -axis directed along the outward normal to the physical surface (i.e. to the local zenith), and  $y$ -axis completing the right-handed orthogonal system. Then the unit vector directed to the Sun has a simple form

$$\mathbf{s} = \begin{pmatrix} s_{\odot} \\ 0 \\ \mu_{\odot} \end{pmatrix}, \quad (1)$$

depending only on the solar zenith distance through its cosine  $\mu_{\odot}$  and sine

$$s_{\odot} = \sqrt{1 - \mu_{\odot}^2}. \quad (2)$$

If the Sun is located at the distance  $R_{\odot}$ , the *collimated radiation flux density* (power per normal area perpendicular to  $s$ ) arriving from the point  $R_{\odot}s$  is

$$J = J_0 \left( \frac{R_0}{R_{\odot}} \right)^2, \quad (3)$$

where the Solar constant  $J_0 \approx 1366 \text{ W m}^{-2}$  is defined for nominal distance  $R_0 = 1 \text{ au}$ . *Irradiance* or *insolation*  $E$  of an arbitrarily oriented surface element is the ratio of the incident power flux  $d\Phi_1$  to the physical area  $dS$ . Accounting for the area projection factor  $\mathbf{s} \cdot \mathbf{n} = \mu_{\odot}$ , where  $\mathbf{n}$  is the unit vector directed to zenith, we can write

$$E(s) = \frac{d\Phi_1}{dS} = \nu J \mu_{\odot}. \quad (4)$$

The visibility function  $\nu$  is either 1, when the Sun is visible at  $dS$ , or 0, when the Sun is occluded.

### 2.2 Bidirectional scattering

Incident radiant power  $d\Phi_1 = E dS$  is partially absorbed (converted into heat) and partially reflected in various directions  $\mathbf{o}$

$$\mathbf{o} = \begin{pmatrix} \sqrt{1 - \mu'^2} \cos \phi \\ \sqrt{1 - \mu'^2} \sin \phi \\ \mu' \end{pmatrix}, \quad (5)$$

where  $\mu$  is the cosine of the zenith distance and  $\phi$  is the azimuth angle in LSF. The cosine of the phase angle between  $s$  and  $\mathbf{o}$  will be designated  $\mu'$ , and defined as the scalar product

$$\mu' = \mathbf{s} \cdot \mathbf{o} = s_{\odot} \sqrt{1 - \mu'^2} \cos \phi + \mu_{\odot} \mu'. \quad (6)$$

The power flux  $d^2\Phi_r$  scattered from  $dS$  into a solid angle  $d\Omega$  in direction  $\mathbf{o}$  is described by *reflected radiance*  $L_r$

$$L_r(\mathbf{o}) = \frac{d^2\Phi_r}{\mu dS d\Omega}, \quad (7)$$

where  $\mu dS$  is the normal surface perpendicular to  $\mathbf{o}$ . Writing  $L_r(\mathbf{o})$  we should bear in mind an implicit dependence on the Sun direction  $s$ , because the reflected power depends on the incident flux from the Sun as well. This dependence becomes more explicit, when we introduce a bidirectional reflectance distribution function (BRDF)  $f_r$  defined as the ratio of the radiance  $L_r$  reflected in the direction  $\mathbf{o}$  to the irradiance  $E$  from the energy source located in the direction  $s$

$$f_r(s, \mathbf{o}) = \frac{L_r(\mathbf{o})}{E(s)}. \quad (8)$$

Although a bidirectional reflectance (BDR) function  $\rho$

$$\rho(s, \mathbf{o}) = \mu_{\odot} f_r(s, \mathbf{o}), \quad (9)$$

seems to be more common in planetary photometry than BRDF, we choose  $f_r$  as a more convenient quantity offering, for example, the reciprocity relation  $f_r(s, \mathbf{o}) = f_r(\mathbf{o}, s)$ . Using Eq. (8) we can express the reflected radiance as

$$L_r(\mathbf{o}) = f_r(s, \mathbf{o}) E(s) = \nu f_r(s, \mathbf{o}) \mu_{\odot} J. \quad (10)$$

Recalling for the reference a traditional, Lambertian BRDF with albedo  $A$

$$f_L = \frac{A}{\pi}, \quad (11)$$

we adopt the anisotropic BRDF proposed by Hapke, namely its version from (Hapke 2002) without macroscopic roughness effects

$$f_r(s, \mathbf{o}) = \frac{w}{4\pi(\mu_{\odot} + \mu)} [(1 + B)P + H(\mu_{\odot})H(\mu) - 1], \quad (12)$$

where the Henyey-Greenstein particle phase function is

$$P = (1 - g^2) [1 + 2g\mu' + g^2]^{-\frac{3}{2}}, \quad (13)$$

and the opposition surge function  $B$  is defined as

$$B = B_0 \left[ 1 + \frac{1}{h} \sqrt{\frac{1 + \mu'}{1 - \mu'}} \right]^{-1}, \quad (14)$$

with

$$B_0 = \frac{S_0 (1 + g)^2}{w (1 - g)}. \quad (15)$$

The Chandrasekhar multiple scattering function  $H$  is defined in terms of an integral equation (Chandrasekhar 1950), but we use the explicit second order approximation given by Hapke (2002)

$$H(x) = \left[ 1 - wx \left( r_0 + \frac{1 - 2r_0 x}{2} \ln \frac{1 + x}{x} \right) \right]^{-1}, \quad (16)$$

where

$$r_0 = \frac{1 - \sqrt{1-w}}{1 + \sqrt{1-w}}. \quad (17)$$

Thus, apart from the incoming and scattered flux directions  $s$  and  $\boldsymbol{o}$ , the Hapke BRDF depends on four physical parameters of the surface: single scattering albedo  $w$ , regolith compaction parameter  $h$ , the opposition surge amplitude  $S_0$  (sometimes replaced by  $B_0$ ), and the asymmetry factor of the Henyey-Greenstein function  $g$ . A more recent version of reflectance was proposed by Hapke (2008); the modification amounts to adding the dependence on porosity as a multiplicative factor in  $f_r$  and a divisor in the argument of  $H$ . This modification is easy to implement, but we suspend its use until controversies concerning the dependence of the opposition effect on porosity are resolved (Hapke 2008).

The total power flux  $\Phi_e$  emitted into the hemisphere

$$\Omega_+ = \{(\mu, \phi) : 0 \leq \mu \leq 1, 0 \leq \phi < 2\pi\},$$

divided by the emitting physical area is termed *radiant exitance*  $M$

$$M = \frac{d\Phi_e}{dS}. \quad (18)$$

Recalling the definition (7), we find for the exitance due to scattering

$$M_r = \int_{\Omega_+} \frac{d^2\Phi_r}{dS d\Omega} d\Omega = \int_{\Omega_+} L_r(\boldsymbol{o}, s) \mu d\Omega. \quad (19)$$

But, according to Eq. (8), radiance is related to irradiance by the BRDF  $f_r$ , hence

$$M_r(s) = E(s) \int_{\Omega_+} f_r(s, \boldsymbol{o}) \mu d\Omega, \quad (20)$$

and the dependence on the Sun location  $s$  appears explicitly.

At this point we can introduce the notion of hemispheric albedo  $A_h$  as the ratio

$$A_h(\mu_\odot) = \frac{M_r}{E(s)}. \quad (21)$$

Combining Eqs. (20) and (21) we see that

$$A_h(\mu_\odot) = \int_{\Omega_+} f_r(s, \boldsymbol{o}) \mu d\Omega = \int_0^{2\pi} d\phi \int_0^1 f_r(s, \boldsymbol{o}) \mu d\mu, \quad (22)$$

and Eq. (20) is simplified to

$$M_r(s) = E(s) A_h(\mu_\odot). \quad (23)$$

For a given set of Hapke parameters the integral (22) can be evaluated numerically on a sufficiently dense set of  $\mu_\odot$  values, allowing to construct an appropriate approximating function. Using the least squares adjustment we construct

$$\mu_\odot A_h(\mu_\odot) \approx A_B \mu_\odot + \alpha_1 \mu_\odot \frac{1 - \alpha_2 \mu_\odot}{1 + \alpha_3 \mu_\odot}, \quad (24)$$

where the Bond albedo  $A_B$ , defined as

$$A_B = \frac{1}{\pi} \int_{\Omega_+} A_h(\mu_\odot) \mu_\odot d\Omega_\odot = 2 \int_0^1 A_h(\mu_\odot) \mu_\odot d\mu_\odot, \quad (25)$$

is the mean slope of the product  $\mu_\odot A_h$ , and the coefficients  $\alpha_i$  of a simple rational approximation describe the deviation from the linear model. We focus on the properties of  $\mu_\odot A_h$ , because in next sections the hemispheric albedo will always appear multiplied by the cosine of the Sun's zenith distance. Note, that the adjustment of  $A_h(\mu_\odot)$  leads to different values of  $\alpha_i$ , degrading the quality of approximation of the product  $\mu_\odot A_h$ .

### 2.3 Geometric albedo

Although the geometric (or physical) albedo is not directly involved in the computation of radiation recoil force, we need it to select an appropriate value of  $w$  for the Hapke model, since usually the observations provide for an asteroid only the geometric albedo and the spectral type.

Let us begin with the notion of *intensity*  $I$ . In contrast to the previously discussed quantities, intensity refers to the power  $d\Phi$  emitted from the whole body surface (not only from an infinitesimal  $dS$ ) in some direction  $\hat{\boldsymbol{q}}$ , divided by the solid angle  $d\Omega$  centered at  $\hat{\boldsymbol{q}}$

$$I(\hat{\boldsymbol{q}}) = \frac{d\Phi}{d\Omega}. \quad (26)$$

The geometric albedo  $p$  is the ratio of observed intensity of some presumably spherical object to the intensity of Lambertian disk with the same diameter as the assumed sphere – both observed from the direction to the Sun, i.e. with zero phase angle. This leads to the integral definition

$$p = 2\pi \int_0^1 \mu_\odot^2 f_r(s, s) d\mu_\odot. \quad (27)$$

Verbisser & Veverka (1995) provide expressions that allow to compute Hapke parameters  $h$ ,  $B_0$ ,  $g$  for various spectral types as functions of a given geometric albedo  $p$  and the mean slope parameter  $G$  of the IAU two-parameter magnitude system (Bowell et al. 1989).

### 2.4 Directional thermal emission

The energy leaving a surface element  $dS$  does not consist only of scattered radiation. If the element has temperature  $T > 0$ , it also emits thermal radiation. Radiant exitance  $M_b$  through  $\Omega_+$  for a black body is given by the Stefan-Boltzmann law

$$M_b = \frac{d\Phi_b}{dS} = \sigma T^4, \quad (28)$$

where  $\sigma = 5.67 \times 10^{-8} \text{ W m}^{-2} \text{ K}^{-4}$ , is the Stefan-Boltzmann constant, and  $\Phi_b$  is the black body value of a more general thermal radiation power flux  $\Phi_t$ . The point black body radiation is by definition isotropic, whereas a black body surface radiation is Lambertian, so the associated radiance  $L_b(\boldsymbol{o})$  in the direction  $\boldsymbol{o}$  is obtained from the general definition of a *thermally emitted radiance*  $L_t$  analogous to (10)

$$L_t(\boldsymbol{o}) = \frac{d^2\Phi_t}{\mu dS d\Omega}, \quad (29)$$

dividing the exitance  $M_b$  by the ‘ $\mu$ -averaged’ solid angle of a hemisphere  $\pi$

$$L_b = \frac{M_b}{\pi}. \quad (30)$$

Indeed, using (30) and the definition of exitance, we verify that

$$\int_{\Omega_+} L_b \mu d\Omega = M_b. \quad (31)$$

*Hemispheric emissivity*  $\epsilon_h$  is defined as the ratio of actual thermal exitance  $M_t$  to the black body exitance  $M_b$

$$\epsilon_h = \frac{M_t}{M_b}. \quad (32)$$

This global quantity should not be confused with a *directional emissivity*  $\epsilon(\boldsymbol{o})$ , defined as the ratio of radiances

$$\epsilon(\mathbf{o}) = \frac{L_t(\mathbf{o})}{L_b(\mathbf{o})}. \quad (33)$$

Directional emissivity plays the role similar to that of BRDF in scattering, although their definitions essentially differ: the former is dimensionless ratio of two radiances, while the latter (with dimension  $\text{sr}^{-1}$ ) is the ratio of radiance to irradiance. So, the thermally emitted radiance in the direction of  $\mathbf{o}$  can be expressed as

$$L_t(\mathbf{o}) = \epsilon(\mathbf{o}) L_b(\mathbf{o}) = \frac{\epsilon(\mathbf{o})}{\pi} \sigma T^4. \quad (34)$$

In present study we adopt the directional emissivity function of Hapke (Hapke 1993; Lagerros 1996)

$$\epsilon(\mu) = \sqrt{1-w} H(\mu), \quad (35)$$

where  $w$  is Hapke's single scattering albedo, and the Chandrasekhar function  $H$  is given by Eq. (16). Thus the emitted radiance is

$$L_t(\mathbf{o}) = \epsilon(\mu) \frac{\sigma T^4}{\pi} = \frac{\sqrt{1-w}}{\pi} H(\mu) \sigma T^4. \quad (36)$$

The exitance  $M_t$  resulting from Eq. (36) is

$$M_t = \int_{\Omega_+} L_t(\mathbf{o}) \mu d\Omega. \quad (37)$$

Confronting it with the primary definition of  $\epsilon_h$  (32), we can use the relation

$$M_t = \epsilon_h \sigma T^4, \quad (38)$$

which leads to the integral expression of hemispheric emissivity

$$\epsilon_h = \int_{\Omega_+} \frac{\epsilon(\mu)\mu}{\pi} d\Omega = 2 \int_0^1 \epsilon(\mu)\mu d\mu, \quad (39)$$

evaluating to a single number for a given set of Hapke parameters.

The infrared radiation of asteroids is often related with the notion of beaming effect, empirically accounted for by the beaming factor  $\eta$  (Lebofsky & Spencer 1989; Lagerros 1996). We do not introduce the beaming factor in our model for a number of reasons: i) the part of beaming that depends on grain size scale radiation transfer should be present in the emissivity function of Hapke, ii) the contribution of thermal lag to the beaming factor is present in the surface temperature model with conductivity, iii) larger scale radiation exchange contribution (Lagerros 1998) will be included in future extensions of our model together with optical interreflections.

## 2.5 Energy balance

Conservation of energy implies, that the total power scattered, thermally re-emitted, and conducted inside the body, should be equal to the incident power flux  $\Phi_i$ . In terms of power density (per physical surface) it means that

$$E(s) = M_r(s) + M_t - Q, \quad (40)$$

i.e. irradiance  $E$  is equal to the sum of total radiant exitance  $M$  and of the conducted heat flux density ( $-Q$ ). Given a nonzero surface conductivity  $K$ , we have

$$Q = -K \mathbf{n} \cdot \nabla T, \quad (41)$$

and then

$$E(s) = A_h(\mu_\odot) E(s) + \epsilon_h \sigma T^4 + K \mathbf{n} \cdot \nabla T, \quad (42)$$

or

$$\epsilon_h \sigma T^4 = \nu \mu_\odot (1 - A_h(\mu_\odot)) J + Q. \quad (43)$$

If  $K = 0$ , Eq. (43) directly provides the surface temperature, generalizing the usual Lambertian Rubincam approximation of the YORP effect to the Hapke reflectance/emissivity model. With  $K \neq 0$ , Eq. (43) serves as a boundary condition for the heat conduction problem.

## 3 RADIATION RECOIL FORCE AND TORQUE

### 3.1 Force expression

Photon flux, leaving  $dS$  in direction  $\mathbf{o}$ , carries energy and momentum (energy divided by the velocity of light  $c$ ), inducing the recoil force  $\mathbf{F}$  equal to the time derivative of momentum and directed opposite to  $\mathbf{o}$ . The force can be easily expressed in terms of emitted radiance, provided we introduce a *radiance vector*

$$\mathbf{L}(\mathbf{o}) = L(\mathbf{o}) \mathbf{o}, \quad (44)$$

where  $L$  is the sum of scattered  $L_r$  and thermal  $L_t$ . The definition of radiance implies that the force density in the direction  $\mathbf{o}$  per physical area and solid angle is

$$\frac{d^2 \mathbf{F}}{dS d\Omega} = -\frac{d^2(\Phi_r + \Phi_t)}{dS d\Omega} \frac{\mathbf{o}}{c} = -\frac{\mu}{c} \mathbf{L}(\mathbf{o}). \quad (45)$$

Integrating over the hemisphere  $\Omega_+$ , we find the net force per physical area

$$\frac{d\mathbf{F}}{dS} = -\frac{1}{c} \int_{\Omega_+} \mu \mathbf{L}(\mathbf{o}) d\Omega. \quad (46)$$

Substituting the expressions (10) and (34), we have

$$\frac{d\mathbf{F}}{dS} = -\frac{1}{c} \int_{\Omega_+} \mu \left( f_r(s, \mathbf{o}) E(s) + \frac{\epsilon(\mu)}{\pi} \sigma T^4 \right) \mathbf{o} d\Omega, \quad (47)$$

or, observing the independence of directional emissivity on azimuth

$$\frac{d\mathbf{F}}{dS} = -\frac{E(s)}{c} \int_{\Omega_+} \mu f_r(s, \mathbf{o}) \mathbf{o} d\Omega - \frac{2\sigma T^4}{c} \int_0^1 \mu^2 \epsilon(\mu) d\mu. \quad (48)$$

Using LSF we can conveniently decompose the force density into the sum of two perpendicular components along the axes  $z$  and  $x$ , i.e. along the surface normal  $\mathbf{n}$  and the unit vector  $\mathbf{m}$

$$\mathbf{n} = \begin{pmatrix} 0 \\ 0 \\ 1 \end{pmatrix}, \quad \mathbf{m} = \begin{pmatrix} 1 \\ 0 \\ 0 \end{pmatrix}. \quad (49)$$

In an arbitrary reference frame we can compute  $\mathbf{m}$  as

$$\mathbf{m} = (s - \mu_\odot \mathbf{n}) s_\odot^{-1}, \quad (50)$$

taking  $\mu_\odot = \mathbf{s} \cdot \mathbf{n}$ .

Splitting the first integrand in Eq. (48) into a sum

$$\begin{aligned} \mu f_r(s, \mathbf{o}) \mathbf{o} &= f_r \mu^2 \mathbf{n} + f_r \mu \sqrt{1 - \mu^2} \cos \phi \mathbf{m} \\ &\quad + f_r \mu \sqrt{1 - \mu^2} \sin \phi (\mathbf{n} \times \mathbf{m}), \end{aligned} \quad (51)$$

and recalling that  $f_r(s, \mathbf{o})$  is an even function of azimuth  $\phi$ , hence the last term in Eq. (51) is odd and its integral over  $\Omega_+$  does vanish, we introduce two auxiliary functions

$$I_1(\mu_\odot) = \int_0^{2\pi} d\phi \int_0^1 \mu^2 f_r(s, \mathbf{o}) d\mu, \quad (52)$$

$$I_2(\mu_\odot) = \int_0^{2\pi} d\phi \int_0^1 \mu \sqrt{1 - \mu^2} \cos \phi f_r(s, \mathbf{o}) d\mu, \quad (53)$$

**Table 1.** Sample Hapke parameters and related quantities

	$p = 0.6$ , type E	$p = 0.1$ , type S
$w$	0.856	0.139
$h$	0.044	0.049
$B_0$	0.8576	1.5407
$g$	-0.2459	-0.2593
$A_B$	0.47542	0.046712
$\alpha_1$	0.14550	0.031021
$\alpha_2$	1.5880	1.6968
$\alpha_3$	0.9741	3.6800
$\xi_{10}$	0.09590	0.01212
$\xi_{11}$	-0.03374	0.3383
$\xi_{12}$	2.1268	1.4786
$\xi_{20}$	0.032156	0.006259
$\xi_{21}$	0.42458	0.16050
$\xi$	0.03024	0.00255
$\epsilon_h$	0.58832	0.96905

as well as a coefficient

$$I_3 = 2 \int_0^1 \mu^2 \epsilon(\mu) d\mu, \quad (54)$$

that allow to rewrite the formula (48) as

$$\frac{d\mathbf{F}}{dS} = -\frac{E(s)}{c} [I_1(\mu_\odot) \mathbf{n} + I_2(\mu_\odot) \mathbf{m}] - \frac{I_3 \sigma T^4}{c} \mathbf{n}. \quad (55)$$

Substituting the boundary conditions (42) into (55) we remove the explicit dependence on  $T^4$ , obtaining

$$\frac{d\mathbf{F}}{dS} = -\frac{E(s)}{c} \left[ \left( I_1(\mu_\odot) + I_3 \frac{1 - A_h(\mu_\odot)}{\epsilon_h} \right) \mathbf{n} + I_2(\mu_\odot) \mathbf{m} \right] - \frac{Q I_3}{c \epsilon_h} \mathbf{n}. \quad (56)$$

However, we prefer to rearrange the force expression into a more comprehensive form

$$\frac{d\mathbf{F}}{dS} = -\frac{2}{3} \frac{1 + \xi}{c} [\nu J \mu_\odot + Q] \mathbf{n} + \frac{\nu J}{c} [X_1 \mathbf{n} - X_2 \mathbf{m}], \quad (57)$$

where functions arguments have been omitted for the sake of brevity.

The coefficient

$$\xi = \frac{3}{2} \frac{I_3}{\epsilon_h} - 1, \quad (58)$$

is a small quantity of order  $10^{-2}$  or less. The two functions

$$X_1 = \mu_\odot \left( \frac{A_h I_3}{\epsilon_h} - I_1 \right), \quad (59)$$

$$X_2 = \mu_\odot I_2, \quad (60)$$

also represent a small deviation from the Lambertian model (see Fig. 1 based upon the data from Tab. 1).

In our judgement there is no point in producing excessively accurate approximations of corrections to the Lambertian model, so we use relatively simple functions, found by trial and error,

$$X_1 \approx \xi_{10} \mu_\odot \frac{1 - \mu_\odot - \xi_{11} \mu_\odot^2}{1 + 3\mu_\odot - \xi_{12} \mu_\odot^2}, \quad (61)$$

$$X_2 \approx \xi_{20} \mu_\odot (3 - \xi_{21} \mu_\odot + \mu_\odot^2) \sqrt{\frac{1 - \mu_\odot}{1 + \mu_\odot}}, \quad (62)$$

with coefficients  $\xi_i$  generated by the least squares adjustment to the results of numerical quadratures.

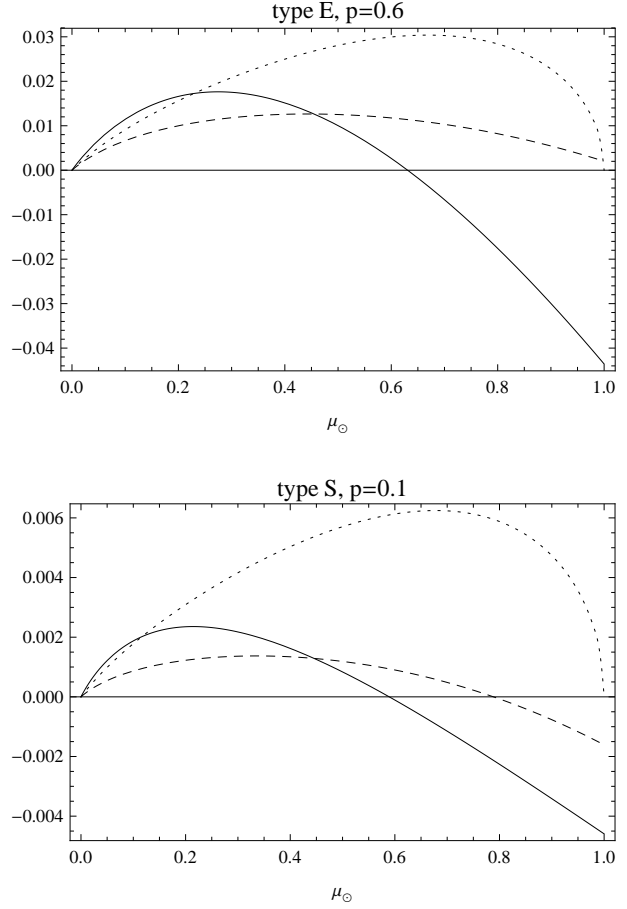


**Figure 1.** Functions describing the non-Lambertian force model. Solid line represents the remainder  $\mu_\odot(A_h - A_B)$ , dashed and dotted lines refer to  $X_1$  and  $X_2$  respectively.

The limit case of Lambertian model results from setting  $\xi = X_1 = X_2 = 0$ , and then Eq. (57) simplifies to

$$\frac{d\mathbf{F}_L}{dS} = -\frac{2}{3c} (\nu J \mu_\odot + Q) \mathbf{n}. \quad (63)$$

Of course, this step also requires assuming a constant  $A_h = A_B$  in boundary conditions (42) for a heat conduction solver providing  $Q$ .

### 3.2 Torque expression

The force defined by Eq. (57) generates for each surface element a torque<sup>1</sup>

$$\begin{aligned} d\mathbf{M} &= \left( \mathbf{r} \times \frac{d\mathbf{F}}{dS} \right) dS = -\frac{2}{3} \frac{1 + \xi}{c} [\nu J \mu_\odot + Q] (\mathbf{r} \times d\mathbf{S}) \\ &\quad + \frac{\nu J}{c} [X_1 (\mathbf{r} \times d\mathbf{S}) - X_2 (\mathbf{r} \times \mathbf{m} dS)]. \end{aligned} \quad (64)$$

The two cross products present in this formula differ in nature; the first, namely

$$\mathbf{r} \times d\mathbf{S} = \mathbf{r} \times \mathbf{n} dS, \quad (65)$$

is constant over time in the body frame, whereas the second,

<sup>1</sup> We maintain the symbol  $\mathbf{M}$  from previous papers hoping that it will not be confused with exitance  $M$  appearing only in Sect. 2.

$$\mathbf{r} \times \mathbf{m} d\mathbf{S} = \frac{\mathbf{r} \times \mathbf{s} - \mu_{\odot} \mathbf{r} \times \mathbf{n}}{s_{\odot}} d\mathbf{S} = \frac{\mathbf{r} \times \mathbf{s}}{s_{\odot}} d\mathbf{S} - \frac{\mu_{\odot}}{s_{\odot}} (\mathbf{r} \times d\mathbf{S}), \quad (66)$$

is time dependent due to the solar motion on local celestial sphere of  $d\mathbf{S}$ .

### 3.3 YORP effect computation

Total YORP torque  $\mathbf{M}$  resulting from the force (57)

$$\mathbf{M} = \oint \left( \mathbf{r} \times \frac{d\mathbf{F}}{d\mathbf{S}} \right) d\mathbf{S}, \quad (67)$$

is obtained by integration over the body surface. The way the integration is handled depends on the type of a body shape model: it can be performed analytically if the surface equation is explicit (e.g. spherical harmonics expansion) or, more often, replaced by the sum over flat faces of a triangulation mesh. In the Rubincam approximation, when  $Q = 0$ , one may simply substitute Eq. (57) into (67) to obtain the torque for a given position of the Sun in the body frame. Most often the resulting torque values are then averaged with respect to rotation and orbital motion in order to extract the secular effects in rotation rate and attitude dynamics. This step requires assumptions about the nominal rotation model that provides the averaging kernel and solar ephemerides.

When the heat conduction is included, the nominal rotation model enters much earlier than in the final averaging: surface temperature oscillations are lagged with respect to the insolation, hence we cannot find  $Q$ , required by the torque formula, without the knowledge of rotation history. Choosing the simplest principal axis rotation mode (known as the gyroscopic approximation) we can easily add non-Lambertian corrections to the algorithm of Breiter et al. (2010) based on a nonlinear 1D thermal model.

The one-dimensional model, where conduction is restricted to the direction normal to the surface, allows a separate treatment of each triangular face of the shape mesh. There, having specified the obliquity  $\varepsilon$  (angle between the spin axis and normal to the orbit) we sample mean anomaly and rotation phase creating the vector of absorbed radiant flux values (the first term in the right-hand side of Eq. (43)). Its discrete Fourier transform (DFT) serves to compute the DFT spectrum of  $Q$  by an iterative process. Once the spectrum of  $Q$  is known, one is able to compute the torque  $\mathbf{M}$ . Until this step, no essential modifications of the algorithm are required; all one has to do is to replace the constant albedo  $A$  (understood as the Bond albedo  $A_B$ ) in the boundary conditions of Breiter et al. (2010) by the hemispheric albedo function  $A_h(\mu_{\odot})$ . Apart from this point, the heat diffusion solver remains practically unchanged; however, computing the mean torque demands a deeper revision. The spectrum of absorbed power flux  $\nu J \mu_{\odot} (1 - A_h)$ , evaluated for the conductivity contribution, cannot be recycled in the Rubincam part, because the hemispheric albedo is not a constant. Thus, outside the conductivity related block, we directly compute the mean values of projections of the Rubincam part  $d\mathbf{M}$  (given by Eq. (64) with  $Q = 0$ ) on unit vectors

$$\begin{aligned} \mathbf{e}_1 &= \sin \Omega' \mathbf{e}_x + \cos \Omega' \mathbf{e}_y, \\ \mathbf{e}_2 &= -\cos \Omega' \mathbf{e}_x + \sin \Omega' \mathbf{e}_y, \\ \mathbf{e}_3 &= \mathbf{e}_z, \end{aligned} \quad (68)$$

where  $\mathbf{e}_x, \mathbf{e}_y, \mathbf{e}_z$  form the body-fixed frame basis, and  $\Omega'$  is the rotation phase measured from the asteroid's equinox (Breiter et al. 2010, prime added to avoid confusion with solid angle  $\Omega$  of the present paper). Then we add the mean values resulting from the DFT spectrum of  $Q$ , obtaining the final averaged torque projections  $\langle M_i \rangle = \langle \mathbf{M} \cdot \mathbf{e}_i \rangle$ .

**Table 2.** Physical and orbital data for the test bodies

		(54509) YORP	(3103) Eger
epoch	JD	2452117.5	2446617.0
semi-axis	au	0.9930	1.4068
eccentricity		0.2305	0.3548
inclination	deg	1.9971	20.939
asc. node	deg	283.835	129.972
arg. perihelion	deg	272.091	253.661
rotation period	h	0.2029	5.7102
ecliptic pole $(\lambda, \beta)$	deg	(180, -85)	(224, -72)
effective diameter	m	113	1778
density	kg m <sup>-3</sup>	2500	2800
conductivity	W m <sup>-1</sup> K <sup>-1</sup>	0.02	0.02
specific heat	J kg <sup>-1</sup> K <sup>-1</sup>	680	680
max. mom. inertia	kg m <sup>2</sup>	$3.04 \times 10^{12}$	$2.80 \times 10^{20}$

If  $\omega$  stands for the rotation rate, the dynamics in the gyroscopic approximation is governed by

$$\dot{\omega} = \frac{M_3}{C}, \quad (69)$$

$$\dot{\varepsilon} = \frac{M_1}{\omega C}, \quad (70)$$

$$\dot{\Omega}' = \omega - \frac{M_2}{\omega C \tan \varepsilon}, \quad (71)$$

where  $C$  designates the maximum moment of inertia in the principal axes frame.

The conclusion of Breiter et al. (2010), that all 1D thermal models imply the independence of the mean period related component  $\langle M_3 \rangle$  on conductivity, holds true regardless of the scattering and emission laws.

## 4 EXEMPLARY RESULTS

In order to see how the improvement of scattering and emission laws affects the simulated YORP effect, we considered two exemplary objects out of the four known to have observationally confirmed spin acceleration: (54509) YORP asteroid with an irregular, radar-determined shape model<sup>2</sup> (Taylor et al. 2007), and (3103) Eger with a convex shape model obtained by lightcurve inversion (Đurech et al. 2009). Both shape models, consisting of 572 (YORP) and 1972 (Eger) triangular facets are displayed in Fig. 2. Orbital and physical parameters assumed in our computations are presented in Table 2. Generally, we tried to maintain coherence with the data applied by Taylor et al. (2007) and Đurech et al. (2009). The effective diameter (the radius of a sphere with the same volume as an object) of Eger was selected indirectly: actually we scaled the asteroid to have the same volume as a spheroid with semi-axes 2.3 and 1.5 km (Benner et al. 1997).

Considering the (54509) YORP, we compared two variants: a realistic assumption that the asteroid is an S-type object with geometric albedo  $p = 0.1$ , and rather fictitious case of spectral type E with  $p = 0.6$ . The Hapke parameters were taken from Table 1. If the Lambert model was assumed, the appropriate Bond albedo

<sup>2</sup> More precisely, we use the 'A-Rough' model available through the NASA PDS website.

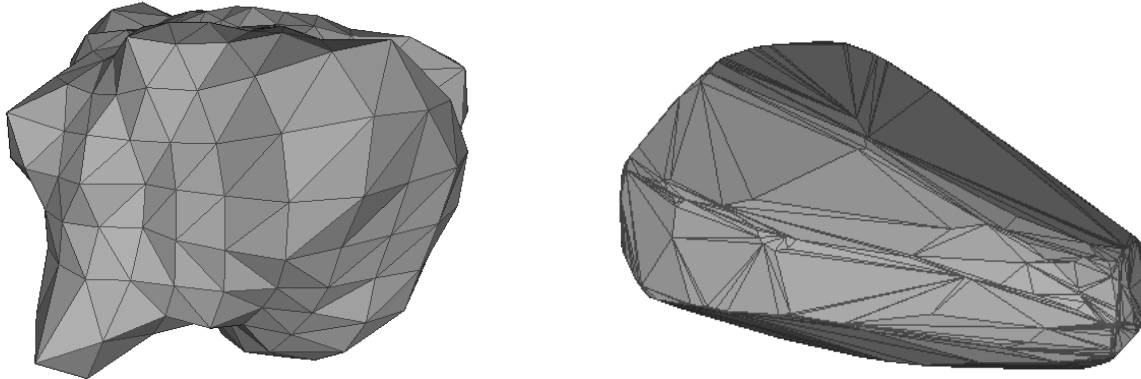


**Figure 2.** Triangulated shape models: left – (54509) YORP, right – (3103) Eger.

and emissivity from Table 1 were applied. For the Lommel-Seeliger model, the single scattering albedo  $w$  was computed from  $A_B$  according to Eq. A3 and the emissivity followed from  $\epsilon_h = 1 - A_B$ . Of course, the Lommel-Seeliger scattering was not considered for  $p = 0.6$  that might lead to hemispheric albedo values outside the  $[0, 1]$  interval.

Figure 3 presents the simulation results for (54509) YORP. Although its caption mentions only Lambert and Hapke models, the Lommel-Seeliger results for  $p = 0.1$  are still there: they practically coincide with the Lambertian solid line. We traced the values of  $\langle M_i \rangle$  for all possible obliquities  $\varepsilon$ , although the actual value for (5409) YORP is  $\varepsilon = 173^\circ$ . The angle between the asteroid’s vernal equinox and the orbital perihelion  $\omega_0$ , irrelevant for the rotation period related  $\langle M_3 \rangle$ , but essential from the point of view of  $\langle M_1 \rangle$  and  $\langle M_2 \rangle$ , responsible for the attitude (Breiter et al. 2010), is  $\omega_0 = 102^\circ$  and we used this value for all  $\varepsilon$  values in Fig. 3. Considering  $\langle M_3 \rangle$  values (Fig. 3, top), we observe that in spite of irregular shape the kind of scattering model at low  $p = 0.1$  has practically no influence on the YORP effect in rotation period, and even at the high albedo case ( $p = 0.6$ ) the difference between Lambert and Hapke models does not exceed 10 percent. The situation is different for  $\langle M_1 \rangle$  and  $\langle M_2 \rangle$ , but there, even for the Lambert model, we have a dependence on albedo resulting from the heat conduction. Although for  $p = 0.1$  there is almost no difference between the Lambert, Lommel-Seeliger, and type S Hapke models, a high geometric albedo  $p = 0.6$  leads to significant differences between the Lambert approximation (dashed) and the E-type Hapke model (dot-dashed). The results for nominal values of  $\varepsilon = 173^\circ$  and  $\omega_0 = 102^\circ$  are collected in Tab. 3. Comparing  $\langle M_3 \rangle$  with the observed  $\dot{\omega} = (4.7 \pm 0.5) \times 10^{-16} \text{ rad s}^{-2}$  (Taylor et al. 2007), we note that the present model overestimates  $\dot{\omega}$  almost 7.6 times, i.e. more than the relevant models used in Taylor et al. (2007). On the other hand, the most significant part of this increase is due to the recomputed reduction to the centre of mass and (more important) principal axes system. If the original body fixed frame is used, we obtain a lower factor 7.0.

In the simulations referring to (3103) Eger we compared only the Lambert and Hapke model for spectral type E with a high geometric albedo  $p = 0.6$ . In spite of a convex shape, excluding all shadowing effects, the dependence of all three  $\langle M_i \rangle$  components on the scattering/emission model has the same relative magnitude as in the case of (54509) YORP. The values for the actual spin axis orientation of Eger are provided in Tab. 4. Interest-

**Table 3.** Mean YORP torques for (54509) YORP at  $\varepsilon = 173^\circ$  and  $\omega_0 = 102^\circ$ . All values in  $10^{-16} \text{ rad s}^{-2}$ .

		$\langle M_1 \rangle$	$\langle M_2 \rangle$	$\langle M_3 \rangle$
Lambert	$p = 0.1$	-0.21	-0.92	35.5
Lommel-Seeliger	$p = 0.1$	-0.18	-0.46	35.4
Hapke (type S)	$p = 0.1$	-0.07	-0.34	34.9
Lambert	$p = 0.6$	-5.07	-6.41	35.5
Hapke (type E)	$p = 0.6$	-4.44	-2.82	32.9

**Table 4.** Mean YORP torques for (3103) Eger at  $\varepsilon = 177^\circ$  and  $\omega_0 = 100^\circ$ . All values in  $10^{-18} \text{ rad s}^{-2}$ .

		$\langle M_1 \rangle$	$\langle M_2 \rangle$	$\langle M_3 \rangle$
Lambert	$p = 0.6$	0.002	-0.93	1.51
Hapke (type E)	$p = 0.6$	0.015	-0.77	1.39

ingly, our modeled values of  $\langle M_3 \rangle$  are very close to the observed  $\dot{\omega} = (1.2 \pm 0.8) \times 10^{-18} \text{ rad s}^{-2}$  reported by Āurech et al. (2009). Of course, this exceptional agreement can be a lucky coincidence, recalling inaccurate nature of photometric convex shape model, roughly estimated density and still a large error margin of the  $\dot{\omega}$  determination.

## 5 CONCLUSIONS

As far as photometry of Solar System bodies is concerned, the bidirectional reflectance model elaborated by Hapke leads to significantly different results than the basic Lambertian framework. But the YORP effect in rotation period occurs to be almost insensitive to the scattering/emission model and even at highest observed albedo values the difference between the two models does not increase to more than 10 percent. However, this low sensitivity should not be interpreted as the evidence of insensitivity of the scattered radiation torque on reflectivity model. Actually, the situation quite opposite. Even for a given Bond albedo value, the part of the YORP torque originating from the recoil of reflected light significantly de-

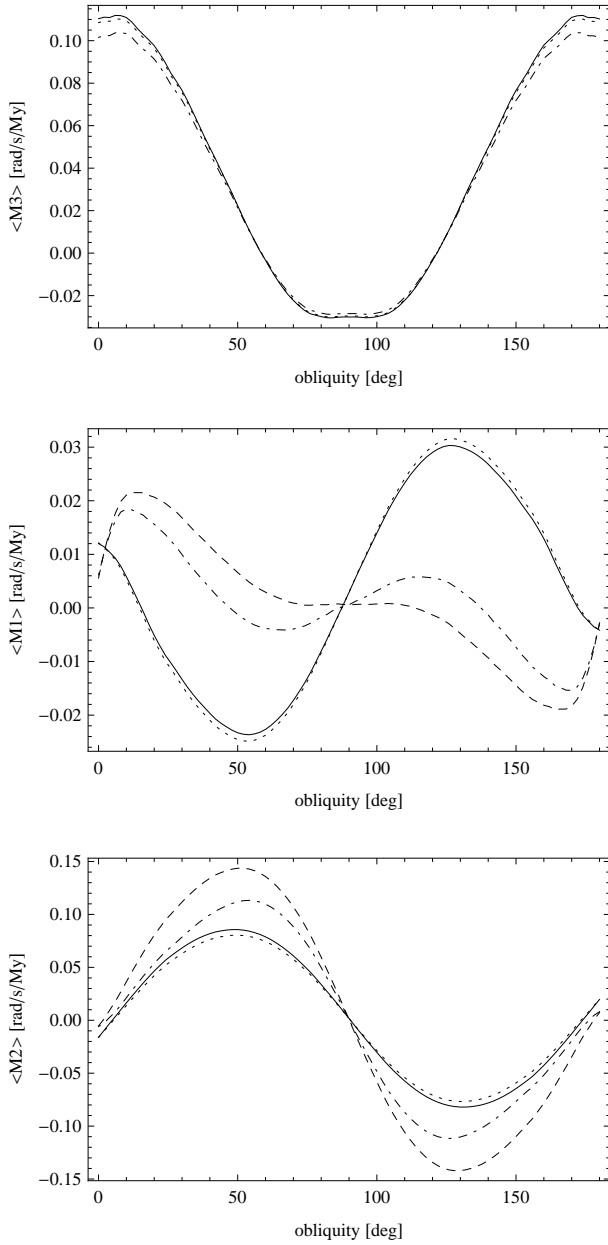


**Figure 3.** Secular YORP effect components on (54509) YORP. Solid line – Lambert type S, dotted – Hapke type S ( $p = 0.1$ ), dashed – Lambert type E, dot-dashed – Hapke type E ( $p = 0.6$ ).

depends on the form of BRDF. But the conservation of energy implies that in the absence of conductivity the sum of scattered and thermally re-radiated energy is always equal to the incident energy. If the hemispheric albedo in some reflection model is higher than the Bond albedo of the Lambert case, more power is scattered, but also less power is thermally re-emitted and vice versa (see Fig. 5). Actually, the same mechanism of energy balance is responsible the independence of YORP on albedo and emissivity in the traditional Rubincam approximation with Lambertian scattering/emission. In the 1D thermal model considered in our paper the  $\langle M_3 \rangle$  component behaves exactly like in the Rubincam’s approximation, so the dependence on reflectance is only due to secondary effects – mostly related with the small deviation of the recoil force from the normal to the surface.

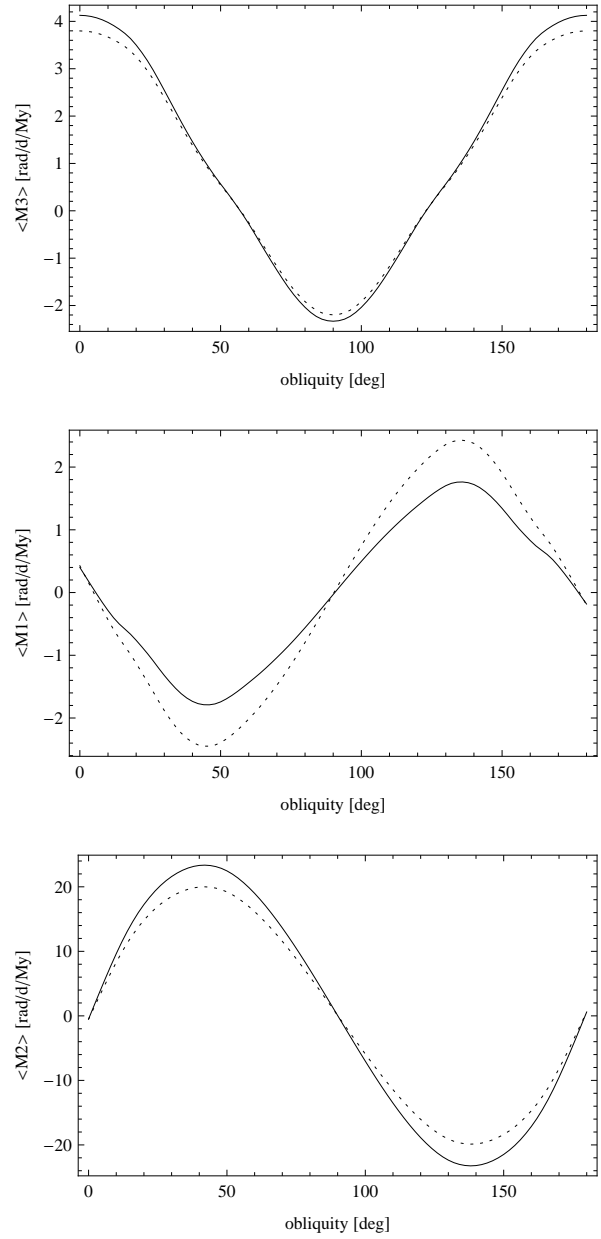


**Figure 4.** Secular YORP effect components on (3103) Eger. Solid line – Lambert type E, dotted – Hapke type E ( $p = 0.6$ ).

Using a more elaborate scattering method is more important in the part of the YORP effect responsible for the orientation of the spin axis. In Rubincam approximation, the situation is similar to that of  $\langle M_3 \rangle$ . But the Rubincam approximation itself is definitely unrealistic for the attitude even at moderate values of conductivity. The influence of heat conduction is proportional to the absorbed fraction of incident energy, hence to the albedo. It means that two scattering models with different dependence of hemispheric albedo on Sun zenith distance will differently affect the balance between scattered and re-radiated power. This explains why using the Hapke BRDF instead of Lambertian model is more important for  $\langle M_1 \rangle$  and  $\langle M_2 \rangle$ , then for  $\langle M_3 \rangle$ .

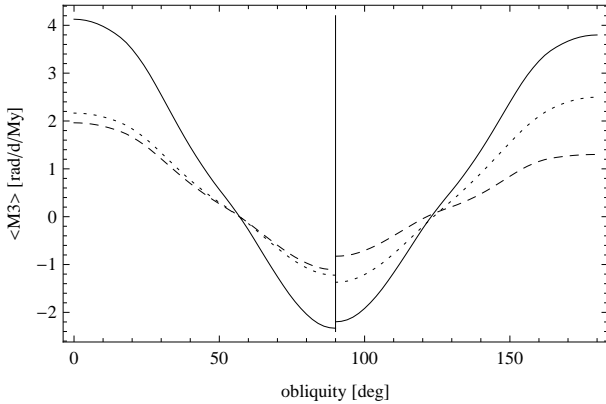


**Figure 5.** YORP effect in  $\omega$  and its components for (3103) Eger. Dashed line – scattered light, dotted – thermal radiation, solid line – total. Left half shows the Lambert case compared with the Hapke model (right half).

## ACKNOWLEDGMENTS

The work of S. Breiter was supported by the Polish Ministry of Science and Higher Education – grant N N203 302535. The work of D. Vokrouhlický was supported by the Czech Grant Agency (grant 205/08/0064) and the Research Program MSM 0021620860 of the Czech Ministry of Education.

## REFERENCES

- Benner L. A. M., et al., 1997, *Icarus*, 130, 296  
 Bowell E., Hapke B., Domingue D., Lumme K., Peltoniemi J., Harris A. W., 1989, in R. P. Binzel, T. Gehrels, & M. S. Matthews ed., *Asteroids II*, pp 524–556  
 Breiter S., Bartczak P., Czekaj M., 2010, *MNRAS*, in press (doi:10.1111/j.1365-2966.2010.17223.x)  
 Breiter S., Bartczak P., Czekaj M., Oczujda B., Vokrouhlický D., 2009, *A&A*, 507, 1073  
 Breiter S., Michalska H., Vokrouhlický D., Borczyk W., 2007, *A&A*, 471, 345  
 Chandrasekhar S., 1950, *Radiative transfer*. Clarendon Press, Oxford  
 Chesley S. R. et al., 2003, *Science*, 302, 1739  
 Čuk M., Burns J. A., 2005, *Icarus*, 176, 418  
 Ďurech J., Vokrouhlický D., Kaasalainen M., et al. 2008, *A&A*, 488, 345  
 Ďurech J., et al., 2008, *A&A*, 489, L25  
 Ďurech J., et al., 2009, in *AAS/Division for Planetary Sciences Meeting Abstracts Vol. 41*, #56.04  
 Fairbairn M. B., 2005, *JRASC*, 99, 92  
 Hapke B., 1981, *JGR*, 86, 4571  
 Hapke B., 1984, *Icarus*, 59, 41  
 Hapke B., 1986, *Icarus*, 67, 264  
 Hapke B., 1993, *Theory of reflectance and emittance spectroscopy*. Cambridge University Press, Cambridge  
 Hapke B., 2002, *Icarus*, 157, 523  
 Hapke B., 2008, *Icarus*, 195, 918  
 Hapke B., Wells E., 1981, *JGR*, 86, 3055  
 Kaasalainen M., Ďurech J., Warner B. D., Krugly Y. N., Gaftonyuk N. M., 2007, *Nature*, 446, 420  
 Lagerros J. S. V., 1996, *A&A*, 310, 1011  
 Lagerros J. S. V., 1998, *A&A*, 332, 1123

- Lebofsky L. A., Spencer J. R., 1989, in R. P. Binzel, T. Gehrels, & M. S. Matthews ed., *Asteroids II*, pp 128–147  
 Lowry S. C., et al., 2007, *Science*, 316, 272  
 Lumme K., Bowell E., 1981, *AJ*, 86, 1694  
 McMahon J., Scheeres D., 2010, *Celestial Mechanics and Dynamical Astronomy*, 106, 261  
 Nesvorný D., Vokrouhlický D., 2008, *A&A*, 480, 1  
 O’Keefe J. A., 1976, *Tektites and their origin*. Elsevier, Amsterdam  
 Paddack S. J., 1969, *J. Geophys. Res.*, 74, 4379  
 Radzievskii V. V., 1954, *Dokl. Akad. Nauk SSSR*, 97, 49  
 Rubincam D. P., 2000, *Icarus*, 148, 2  
 Rubincam D. P., Paddack S. J., 2010, *Icarus*, in press, doi: 10.1016/j.icarus.2010.05.015  
 Scheeres D. J., 2007, *Icarus*, 188, 430  
 Scheeres D. J., Gaskell R. W., 2008, *Icarus*, 198, 125  
 Statler T. S., 2009, *Icarus*, 202, 502  
 Taylor P. A., et al., 2007, *Science*, 316, 274  
 Verbiscer A. J., Veverka J., 1995, *Icarus*, 115, 369  
 Vokrouhlický D., Bottke Jr. W. F., 2001, *A&A*, 371, 350  
 Vokrouhlický D., Chesley S. R., Matson R. D., 2008, *AJ*, 135, 2336  
 Yarkovsky I. O., 1901, *The density of luminiferous ether and the resistance it offers to motion (in Russian)*, Bryansk

## APPENDIX A: LOMMEL-SEELIGER APPROXIMATION

The Lommel-Seeliger scattering law (Fairbairn 2005) is defined by the BRDF

$$f_{LS}(s, \theta) = \frac{w}{4\pi(\mu_{\odot} + \mu)}, \quad (\text{A1})$$

which can be seen as a simplified Hapke model independent on the phase angle  $g$ . Using this simple law we find most of the expressions in exact, closed form, depending on the single scattering albedo  $w$ . The hemispheric albedo is

$$A_h(\mu_{\odot}) = \frac{w}{2} \left( 1 + \mu_{\odot} \ln \frac{\mu_{\odot}}{1 + \mu_{\odot}} \right), \quad (\text{A2})$$

leading to the Bond albedo

$$A_B = \frac{2(1 - \ln 2)}{3} w \approx 0.204569 w, \quad (\text{A3})$$

and the geometric albedo

$$p = \frac{w}{8}. \quad (\text{A4})$$

Note that the last formula leads to problems with  $w > 1$  in Hapke’s thermal radiation expressions if we try to use it for bright objects with  $p > 0.125$ . In these circumstances we combine the Lommel-Seeliger scattering with a Lambertian grey body emission model, imposing  $\xi = 0$ . Then,

$$X_1(\mu_{\odot}) = \frac{w\mu_{\odot}}{12} \left[ 1 + 6\mu_{\odot} + 2\mu_{\odot}(2 + 3\mu_{\odot}) \ln \frac{\mu_{\odot}}{1 + \mu_{\odot}} \right], \quad (\text{A5})$$

and  $X_2 = 0$ . The resulting force per area

$$\frac{d\mathbf{F}}{dS} = -\frac{2}{3c} [vJ\mu_{\odot} + Q] \mathbf{n} + \frac{vJ}{c} X_1 \mathbf{n}, \quad (\text{A6})$$

is directed along the surface normal, similarly to the Lambertian case.

**APPENDIX B: DIRECT RADIATION PRESSURE**

In the usual YORP models of a single, Sun orbiting object the direct radiation pressure, opposite to the Sun vector  $s$ , is either a priori discarded or its effect disappears after the double (rotation and orbit) averaging. However, this phenomenon may play some role when a binary system is studied – most notably for the BYORP effect (Čuk & Burns 2005; McMahon & Scheeres 2010). In such cases, the force and torque should be complemented with following terms:

$$\frac{d\mathbf{F}_d}{dS} = -\frac{\nu J\mu_\odot}{c} \mathbf{s} = -\frac{\nu J\mu_\odot}{c} (\mu_\odot \mathbf{n} + s_\odot \mathbf{m}), \quad (\text{B1})$$

being the addition to Eq. (57), and the resulting torque

$$\frac{d\mathbf{M}_d}{dS} = \mathbf{r} \times \frac{d\mathbf{F}_d}{dS}. \quad (\text{B2})$$

Note that for a binary system the visibility function  $\nu$  additionally involves occultations by the second object.

With these complements, the complete force  $d\mathbf{F}_c = d\mathbf{F} + d\mathbf{F}_d$  acting on a surface element is

$$\begin{aligned} d\mathbf{F}_c = & -\frac{2}{3} \frac{1+\xi}{c} [\nu J\mu_\odot + Q] dS \\ & + \frac{\nu J}{c} \left[ (X_1 - \mu_\odot^2) dS - (X_2 + \mu_\odot s_\odot) m dS \right], \end{aligned} \quad (\text{B3})$$

and the complete torque is readily obtained by the cross product

$$d\mathbf{M}_c = \mathbf{r} \times d\mathbf{F}_c. \quad (\text{B4})$$

Equation (B1) involves an implicit statement that all photons hitting the surface are absorbed and transfer their momentum before being re-emitted in any form, including the one termed reflection. In a perfect specular reflection, all photons arriving from  $\mathbf{s} = \mu_\odot \mathbf{n} + s_\odot \mathbf{m}$ , leave the surface in the symmetric direction  $\mathbf{s}' = \mu_\odot \mathbf{n} - s_\odot \mathbf{m}$ . So, the total effect of perfect specular reflection is

$$d\mathbf{F}_s = -\frac{2\nu J\mu_\odot^2}{c} dS, \quad (\text{B5})$$

with the  $\mathbf{m}$  component canceled. As a consequence, we may interpret the occurrence of function  $X_2$  as a footprint of imperfect specular reflection in the Hapke's model, with only a part of power incoming from  $\mathbf{s}$  leaving the surface along  $\mathbf{s}'$ .